Local interaction simulation approach to modelling nonclassical, nonlinear elastic behavior in solids

Marco Scalerandi,[a] Valentina Agostini, and Pier Paolo Delsanto
INFM, Dip. Fisica, Politecnico di Torino, C.so Duca degli Abruzzi 24, Torino, Italy

Koen Van Den Abeele
Interdisciplinary Research Center, Fac. of Science, K. U. Leuven Campus Kortrijk, E. Sabbelaan 53, B-8500 Kortrijk, Belgium

Paul Allen Johnson
Los Alamos National Laboratory, Nonlinear Elasticity Group, MS D-443, Los Alamos, New Mexico 87545

(Received 16 July 2002; revised 6 February 2003; accepted 10 March 2003)

Recent studies show that a broad category of materials share ''nonclassical'' nonlinear elastic behavior much different from ''classical'' (Landau-type) nonlinearity. Manifestations of ''nonclassical'' nonlinearity include stress–strain hysteresis and discrete memory in quasistatic experiments, and specific dependencies of the harmonic amplitudes with respect to the drive amplitude in dynamic wave experiments, which are remarkably different from those predicted by the classical theory. These materials have in common soft ''bond'' elements, where the elastic nonlinearity originates, contained in hard matter (e.g., a rock sample). The bond system normally comprises a small fraction of the total material volume, and can be localized (e.g., a crack in a solid) or distributed, as in a rock. In this paper a model is presented in which the soft elements are treated as hysteretic or reversible elastic units connected in a one-dimensional lattice to elastic elements (grains), which make up the hard matrix. Calculations are performed in the framework of the local interaction simulation approach (LISA). Experimental observations are well predicted by the model, which is now ready both for basic investigations about the physical origins of nonlinear elasticity and for applications to material damage diagnostics. © *2003 Acoustical Society of America.* [DOI: 10.1121/1.1570440]

PACS numbers: 43.25.Dc, 43.25.Gf, 43.25.Ed [MFH]

I. INTRODUCTION

In the last decade, numerous studies of a diverse class of materials such as earth materials, cement products, concrete, composites, etc., have shown that their elastic nonlinear behavior is significantly different from the classical nonlinear behavior found in ''ordinary'' materials, such as glasses, single crystals, and numerous others.[1–3] Despite their very different structural and chemical properties, these materials share the same nonlinear elastic signatures that can be observed in both quasistatic and dynamic experiments. In the following we shall say that these materials display ''nonclassical'' nonlinearity, while the ''ordinary'' materials, which obey the traditional nonlinear theory of Landau[4,5] shall be called ''classical'' nonlinear.

The fundamental characteristic of nonclassical material behavior in quasistatic experiments is the appearance of stress–strain hysteresis and discrete memory.[6] Differences between nonclassical and classical nonlinear dynamic behavior include: a downshift of the resonance frequency, proportional to the resonance amplitude in the nonclassical case versus a quadratic amplitude dependence in the classical case; nonlinear attenuation versus amplitude independent attenuation; quadratic amplitude dependence of the third harmonic versus cubic in the classical case.[2] Another striking feature observed in the nonclassical nonlinear dynamic response of nonclassical materials is ''slow dynamics,'' i.e., the slow recovery of the linear material properties (wavespeed and attenuation) after a sample has been subjected to a force.[7–9]

Nonclassical nonlinear effects are believed to be due to the presence of soft regions in hard materials (e.g., microcracks, flat pores and soft bonding regions between grains in a granular material). They have been successfully reproduced by a model proposed by Holcombe and, later, by Guyer and McCall,[10] based on a Preisach–Mayergoyz (PM) space representation, in analogy with the treatment of magnetic hysteresis. Such a model provides a simple phenomenological description of the complex elastic behavior of an elementary elastic unit in the composition of an arbitrary material. Each unit is described by an elementary constitutive law that accounts for effects such as nonlinearity, hysteresis and endpoint memory. The collection of all units, each of them with their particular constitutive relations, yields the so called ''PM space,'' which characterizes the material specimen and can be used to predict the static mechanical behavior of rocks in agreement with macroscopic observations. In the case of dynamic problems, Van Den Abeele *et al.*[11] used a quasianalytical approximation of this model for homogeneous and

[a]Author to whom correspondence should be addressed; electronic mail: scalerandi@polito.it

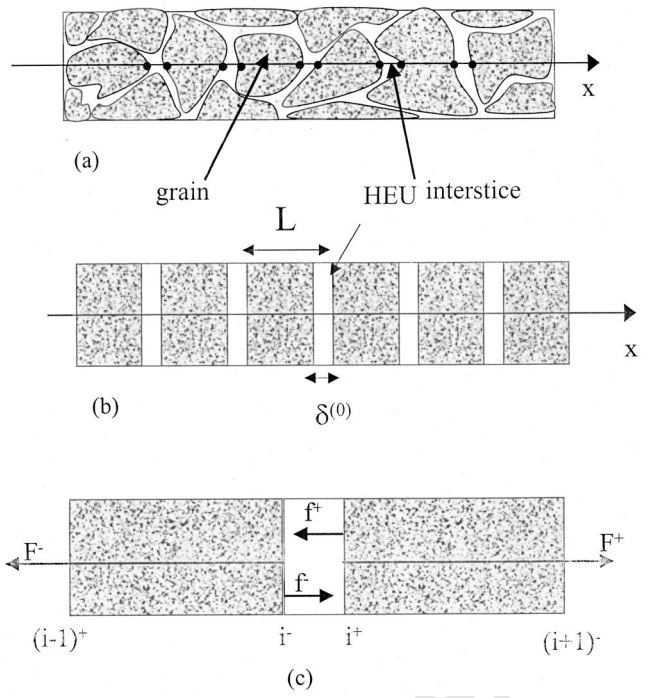

FIG. 1. (a) Representation of a specimen bar with grains and interstices; (b) its 1D schematic representation; (c) representation of the forces acting on the two subnodes delimiting an interstice.

isotropic nonlinear media to evaluate the influence of hysteresis on the propagation of longitudinal waves.

Analytical approaches significantly simplify the problem but may not succeed in reproducing the whole set of observed phenomena. Application of numerical calculations can serve as an alternative for a more complete theoretical analysis, including the extension of a basic one-dimensional model to higher dimensions. Computer models based on a microscopic approach, such as *ab initio* calculations and molecular dynamic techniques[12] are commonly used and allow, for instance, the understanding of atomic-scale effects and material behavior under applied stresses.[13] However, such methods are often of no practical use because of the huge CPU time required, even for simulations over a relatively small number of atoms. Therefore, a bridging between a microscopic and a macroscopic description is extremely useful.

In wave propagation applications, Delsanto *et al.*[14] proposed an approach for numerical simulations of macroscopic wave phenomena in complex heterogeneous media by introducing localized features at the mesoscopic to microscopic scale. The approach is based on the local interaction simulation approach (LISA)[15] in conjunction with a spring model.[16] A very important feature of LISA is, as its name implies, the capability of implementing at the local level even very complex mechanisms, which would be difficult to include in a partial differential equation. In fact the method allows full freedom in the choice of interaction between the nodes which represent the boundaries of the material cells.

It is also possible, by splitting the nodes at the interfaces between different material components into ''subnodes,'' each related to a different component, to include all kinds of microscopic-to-mesoscopic scale features. Such a model was implemented numerically in the LISA framework to simulate the influence of the local nonlinear elastic properties on the one-dimensional dynamic wave propagation in nonclassical materials.[17] To our knowledge, this is the only study to date that explicitly incorporates a macroscopic simulation of dynamic nonlinearity and hysteresis.

One of the drawbacks of numerical simulations is the difficulty of insuring the convergence and stability of the solutions. In this work, we propose a modification of the micromechanical properties of the individual units, as suggested in previous papers,[10] providing both an alternative physical description of the elasticity of the bond system and a more stable numerical treatment.

In Sec. II, we define for each unit the nonanalytical constitutive law provided by the model used as input for the LISA simulation. The main difference with the model of Guyer and McCall[10] is that the units, which represent the interstices between grains, are elastic and therefore not restricted to only two strain states (''open'' and ''closed''). In Sec. III, a generalization of the spring model[16] is introduced for the simulation of the propagation of ultrasonic waves in classical materials, with both rigid and nonrigid interfaces. The approach is then extended to the treatment of nonclassical nonlinearities.

In order to illustrate the applicability of the model, we focus our attention on simulations of a resonant bar experiment (Sec. IV) and show that our model is capable of reproducing all of the observed nonclassical nonlinear features.

II. CONSTITUTIVE RELATIONS

Let us consider a sample of a multigrained material, as shown in Fig. 1(a). For simplicity, we assume that grains are homogeneous and that the distance between two grain centers is L when no pressure is applied to the bar. Likewise we assume that, initially, all the interstices between grains have the same length $\delta^{(0)} \ll L$. The bar may then be represented by the 1D lattice sketched in Fig. 1(b): a sequence of elastic portions separated by soft interstice regions. The latter can be thought of as the bond system between the grains. In the following we will call the combination of elastic grain and interstice elastic unit (EU) or lattice cell.

In the PM space model,[10] the interstice regions can exist only in two states: open or closed. In the open state the interstice has a length δ_0. When the pressure on the interstice increases, it behaves rigidly and remains at the length δ_0 up to a certain pressure P_c. At this pressure level, the interstice instantaneously closes (infinitely soft elasticity for an infinitesimal short time) and assume the length δ_c ($\leqslant \delta_0$). Upon further increase of pressure, the interstice continues to behave rigidly, this time with length δ_c. When decreasing the pressure, the interstice remains at its length δ_c down to a pressure level $P_0 (\leqslant P_c)$, where it instantaneously opens, and remains at the length δ_0 upon further decrease of the pressure. The grains are considered to be purely elastic, represented by a modulus K_g. The corresponding stress–

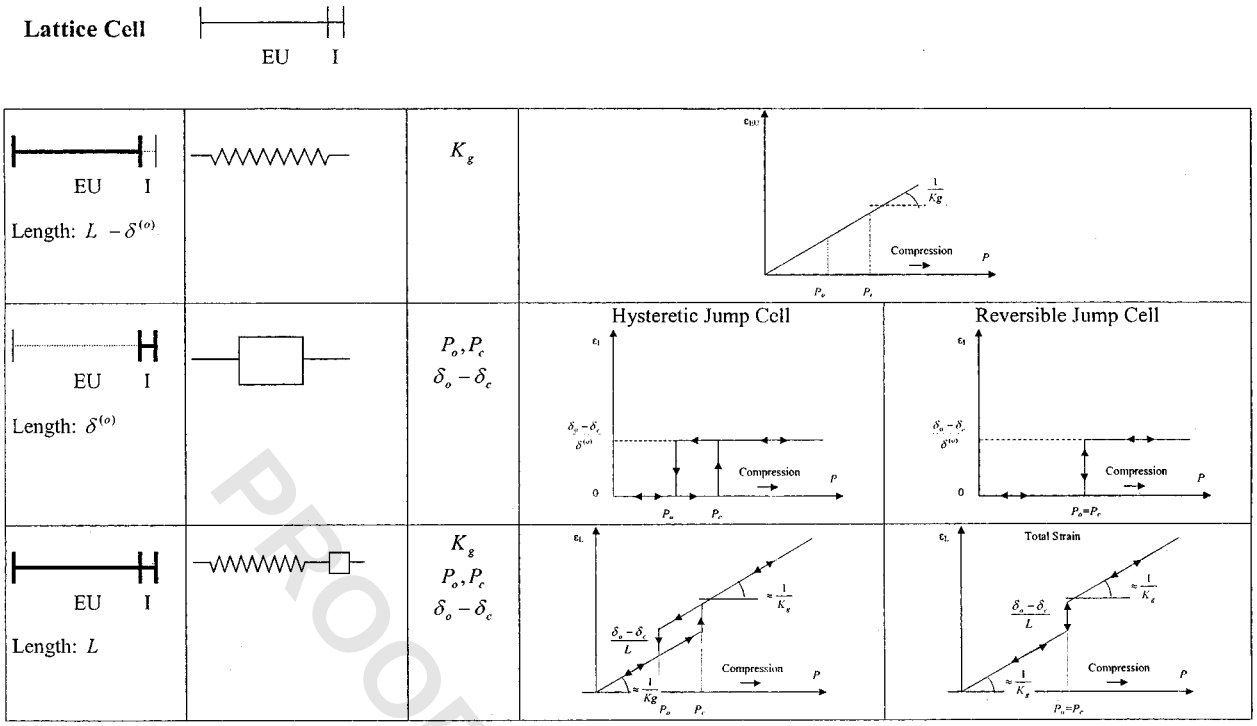

(a)

$$\varepsilon_{EU} = \frac{P}{K_g} \qquad \varepsilon_I = \begin{cases} 0 & \text{if } (P < P_c \text{ and } P \text{ increasing}) \text{ or } (P < P_0 \text{ and } P \text{ decreasing}) \\ \dfrac{\delta_o - \delta_c}{\delta^{(o)}} & \text{if } (P > P_c \text{ and } P \text{ increasing}) \text{ or } (P > P_0 \text{ and } P \text{ decreasing}) \end{cases}$$

$$\varepsilon_L = \frac{L-\delta^{(o)}}{L}\varepsilon_{EU} + \frac{\delta^{(o)}}{L}\varepsilon_I = \frac{L-\delta^{(o)}}{L}\frac{P}{K_g} + \begin{cases} 0 & \text{if } (P < P_c \text{ and } P \text{ increasing}) \text{ or } (P < P_0 \text{ and } P \text{ decreasing}) \\ \dfrac{\delta_o - \delta_c}{L} & \text{if } (P > P_c \text{ and } P \text{ increasing}) \text{ or } (P > P_0 \text{ and } P \text{ decreasing}) \end{cases}$$

$$\text{and thus } \varepsilon_L \approx \frac{P}{K_g} + \begin{cases} 0 & \text{if } (P < P_c \text{ and } P \text{ increasing}) \text{ or } (P < P_0 \text{ and } P \text{ decreasing}) \\ \dfrac{\delta_o - \delta_c}{L} & \text{if } (P > P_c \text{ and } P \text{ increasing}) \text{ or } (P > P_0 \text{ and } P \text{ decreasing}) \end{cases}$$

(b)

FIG. 2. The micromodel of Guyer and McCall (Ref. 10) illustrating the stress–strain behavior of a typical lattice cell composed of an elastic unit and a nonclassical interstice. The grains are purely elastic, the interstices display jump and hysteresis phenomena. Apart from two geometric parameters (L and $\delta^{(0)}$, see Fig. 1), lattice cells are represented by four ''elastic'' parameters: the elasticity of the grains K_g, the opening and closing pressures P_0 and P_c, and the elementary length change $\delta_0 - \delta_c$. The total strain on a lattice cell can be calculated by a series interaction. A statistical ensemble of such cells represents a microinhomogeneous material.

strain relations are shown in Fig. 2 (we consider the strain ϵ to be positive if the length is decreasing, and pressure is considered positive in compression, negative in tension). The pairs (P_0, P_c) have generally different values for each interstice.

The residual modulus of a lattice cell K_{cell} can be calculated as follows:

$$\frac{1}{K_{\text{cell}}} = \frac{1}{K_g} + \frac{1}{K_I}, \tag{1}$$

where K_I is the interstice modulus, which is infinity (rigid behavior) except at P_0 and P_c. For completeness, we also illustrate in Fig. 2 the elastic response of a single lattice cell, both for $P_0 \neq P_c$ (hysteretic jump cell) and for $P_0 = P_c$ (reversible jump cell).[10] Apart from two geometric parameters (L and $\delta^{(0)}$), lattice cells in this model are thus represented by four ''elastic'' parameters: K_g, P_0, P_c, and δ_0.

For numerical simulations, the appearance of jumps in the state equation, i.e., i the interstice length, may cause problems of convergence and stability. Also, from a physical point of view, discontinuities in a physical parameter are unrealistic. Ideally, it would be most satisfactory to describe the elastic behavior by means of smooth analytic functions. As an example, the expressions

$$\epsilon=\begin{cases}\dfrac{P}{K_g}+\dfrac{P+P_0-\chi\ln[\cosh((P-P_0)/\chi)]}{2K_I}+\kappa\left(1+\tanh\left(\dfrac{P-P_0}{\chi}\right)\right) & \text{if } P>0,\\ \dfrac{P}{K_g}+\dfrac{P+P_0-\chi\ln[\cosh((P-P_0)/\chi)]}{2K_I}+\left(\kappa+\dfrac{(P_c-P_0)}{K_I}\right)\left(1+\tanh\left(\dfrac{P-P_0}{\chi}\right)\right) & \text{if } P<0\end{cases} \tag{2}$$

yield the elastic stress-strain behavior of the lattice cell illustrated in Fig. 3, i.e., describes the hysteresis loop. Here, a total of six ''elastic'' parameters are involved: K_g, K_I, P_0, P_c, κ, and χ. K_I introduces a difference in elasticity modulus before and after the hysteretic open-closure pressure range; κ reflects the magnitude of the jump in strain at P_c and χ takes into account the smoothness of the transitions at P_c and P_0. The PM space of Ref. 10 can be reproduced in the limit of $K_I\to\infty$ and $\chi=0$, i.e., when there is no change in the elasticity modulus before and after closure, and the closing and opening are instantaneous in pressure.

However, since we are treating the bond system as soft inclusions, it is reasonable to assume that the modulus of a lattice cell alters when the elastic features change states. Therefore, it seems appropriate to retain the interstice softness parameter K_I at a value different from infinity. In order to limit the number of free parameter values to four, as in the original PM space model, we put $\kappa=\chi=0$. In doing so, we have adjusted the micromechanical properties of the bond elements, introducing a state variable which rules the interstice elastic properties. Instead of opening and closing discontinuously in pressure, the interstice element behaves linearly elastic, with modulus $K'=\delta^{(0)}/L^{(0)}K_I$, up to the pressure P_c. At that pressure level, the element becomes rigid (infinite modulus), and it remains rigid for all pressures above. When decreasing the pressure, the interstice remains at a fixed length down to a pressure level P_0, where it instantaneously opens and continues afterwards to increase its length according to Hooke's law,

$$\epsilon_I=\frac{\delta^{(0)}-\delta}{\delta^{(0)}}=\frac{P}{K'}. \tag{3}$$

The sudden decrease in strain (increase in length) of the lattice cell at P_0 amounts to $(P_c-P_0)/K_I$. The corresponding stress–strain behavior of the elastic unit, the interstice element and the total lattice cell are shown in Fig. 4. As in the case of the original PM space model, the micromechanical behavior can be described by piecewise linear functions. If $P_0=P_c$, we talk of a reversible elastic unit (REU). If P_0 differs from P_c, we use the term hysteretic elastic unit (HEU).

The new representation is an alternative model to the PM space model for a possible nonclassical physical mechanism. Of course, the choice of the protocol for the state variable should be dictated by the physical processes involved in the propagation at a microscopic level (work in progress). However, the simple phenomenological protocol used here already yields satisfactory results. It also has the advantage of eliminating the discontinuities of the physical parameter by replacing them with two discontinuities of a state variable, to be defined in the next section. This is important for the stability and convergence of the simulations. In the following section, we implement this type of elastic behavior in the framework of the local interaction simulation approach (LISA). However, the LISA approach can be applied to evaluate the macroscopic dynamic response of systems with any type of local nonclassical nonlinear elasticity.[17] In the present paper, first we consider the case of ''classical phase'' materials with completely rigid bonds, then we introduce linearly elastic bonds, and finally we implement the case of bonds with the assumed nonlinear elasticity, in order to describe the macroscopic dynamic behavior of nonclassical materials.

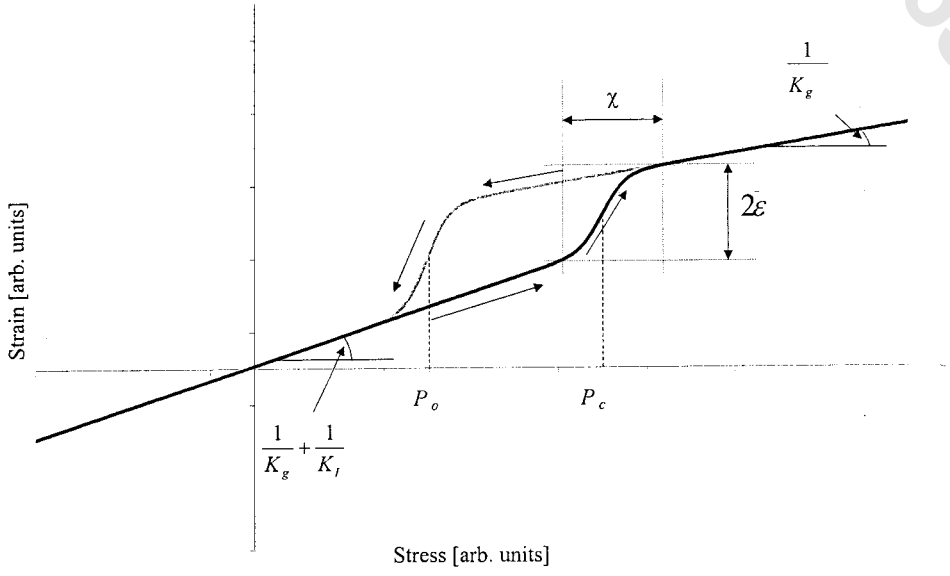

FIG. 3. A continuous micromodel illustrating the stress–strain behavior of a lattice cell characterized by a set of six ''elastic'' parameters: K_g, K_I, P_0, P_c, κ, and χ.

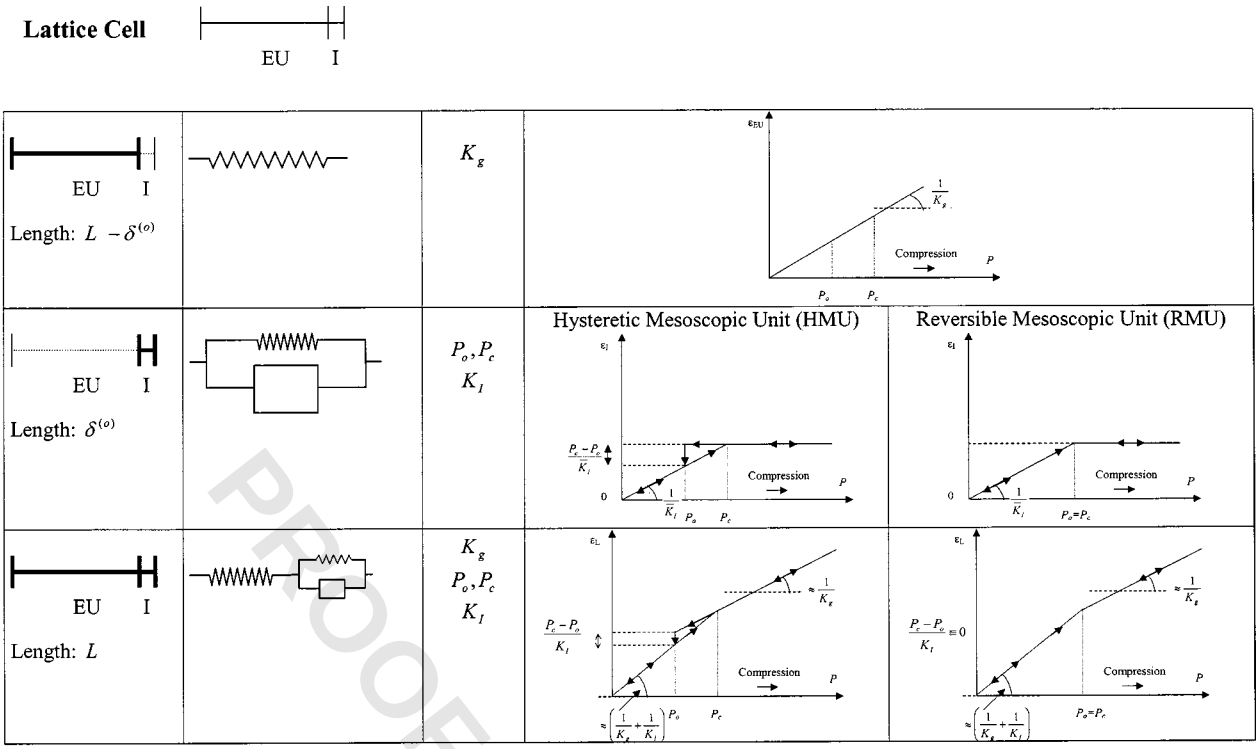

(a)

$$\varepsilon_{EU} = \frac{P}{K_g} \qquad \varepsilon_I = \begin{cases} \dfrac{P}{K_I} & \text{if } (P < P_c \text{ and } P \text{ increasing}) \text{ or } (P < P_0 \text{ and } P \text{ decreasing}) \\ \dfrac{P_c}{K_I} & \text{if } (P > P_c \text{ and } P \text{ increasing}) \text{ or } (P > P_0 \text{ and } P \text{ decreasing}) \end{cases}$$

$$\varepsilon_L = \frac{L-\delta^{(o)}}{L}\varepsilon_{EU} + \frac{\delta^{(o)}}{L}\varepsilon_I = \frac{L-\delta^{(o)}}{L}\frac{P}{K_g} + \begin{cases} \dfrac{\delta^{(o)}}{L}\dfrac{P}{K_I} = \dfrac{P}{K_I} & \text{if } (P < P_c \text{ and } P \text{ increasing}) \text{ or } (P < P_0 \text{ and } P \text{ decreasing}) \\ \dfrac{\delta^{(o)}}{L}\dfrac{P_c}{K_I} = \dfrac{P_c}{K_I} & \text{if } (P > P_c \text{ and } P \text{ increasing}) \text{ or } (P > P_0 \text{ and } P \text{ decreasing}) \end{cases}$$

$$\text{and thus } \varepsilon_L \approx \frac{P}{K_g} + \begin{cases} \dfrac{P}{K_I} & \text{if } (P < P_c \text{ and } P \text{ increasing}) \text{ or } (P < P_0 \text{ and } P \text{ decreasing}) \\ \dfrac{P_c}{K_I} & \text{if } (P > P_c \text{ and } P \text{ increasing}) \text{ or } (P > P_0 \text{ and } P \text{ decreasing}) \end{cases}$$

(b)

FIG. 4. The currently used micromodel illustrating the stress–strain behavior of a typical lattice cell composed of a purely elastic unit and a nonclassical interstice displaying both elasticity and jump and hysteretic phenomena. Apart from the geometric parameters, the lattice cells in this model are represented by four "elastic" parameters: the elasticity of the grains K_g, the opening and closing pressures P_0 and P_c, and the elasticity of the interstices K_I. The total strain on a lattice cell can be calculated by a series interaction. This micromodel derives from the general continuous model by setting both κ and χ equal to zero.

III. THE LISA MODEL

As shown in Fig. 1, each lattice cell consists of an elastic portion (grain) and an interstice element (bond). According to our model, the latter is responsible for the elastic hysteretic response. In order to describe the interstice region between two grains, each grid node i is split into two subnodes $i^{\pm}$ [see Fig. 1(c)]. Since in dynamical experiments the contribution of classical nonlinearity is generally negligible, we assume that the grains are linearly elastic. We confine all the nonlinear behavior to the interstices. Associated with each subnode is a length $L_n = L/2$ (i.e., of half a grain) and a mass $m_n = \rho L_n$, where ρ is the mass density per unit length. The interstices are considered to have zero mass (because $\delta^{(0)}$ is assumed to be very small). We call the combination of two subnodes left and right of a grid node, with their lengths and masses, a GBG cell (grain–bond–grain). Depending on the elastic behavior of the grains and the bond, this cell can be linearly elastic, classical nonlinear or nonclassical nonlinear.

For the simulation of dynamic processes, we also consider a time discretization $t = 0,1,2,...$ with a constant time step τ. When referring to lengths (δ), displacements (u) and forces (F, f), the first subscript always refers to the space discretization, whereas the second refers to the time discretization. However, for brevity, starting with Eq. (3), we will

usually omit one or both indices when equal to the ''current'' values of i and/or t.

A. Classical phase materials

Classical phase materials are elastic materials with a classical bond system, i.e., the elastic behavior of both grains and bonds is linear or classically nonlinear. A particular case occurs when all of the interstices behave rigidly, i.e., the length of each interstice remains constant:

$$\delta_{i,t}=\delta_i^{(0)}+u_{i,t}^{+}-u_{i,t}^{-}=\text{const} \quad \forall T_0\leqslant t\leqslant T_1, \tag{4}$$

where T_0 and T_1 represent two arbitrary times and $\delta_i^{(0)}$ is the rest length of the ith interstice. This corresponds to the case of ''perfect contact'' in Ref. 16. In other cases of ''classical phase elasticity'' $\delta_{i,t}$ may be allowed to vary, provided the elastic modulus (i.e., the derivative of the stress with respect to the strain) is a continuous (linear or nonlinear) function of the applied stress.

To describe the general case, we assume that the following forces act on each subnode (we use the convention that forces are positive when pointing to the positive x direction):

An ''external'' elastic force $F_{i,t}^{\pm}$, due to the presence of an excitation of the bar at the interstice i at the time t. Neglecting, as mentioned, the classical nonlinear terms,

$$F_{i,t}^{\pm}=K_g\frac{u_{i\pm1,t}^{\mp}-u_{i,t}^{\pm}}{L}, \tag{5}$$

where K_g is the stiffness of the grains and $u_{i,t}^{\pm}$ is the subnode displacement.

A ''dissipative'' force $\gamma\, du_{i,t}^{\pm}/dt$, which is required in the simulation of dynamic resonance experiments in order to obtain steady state solutions.

An ''internal'' force, which acts on the interstice to keep the two subnodes together and transmits the external excitation through the bar.[16] Since the interstice itself has no mass: $f_{i,t}^{+}=-f_{i,t}^{-}$. These forces represent the ''interaction forces'' in the interstice.

An elastic ''restoring'' force

$$\mathfrak{I}_{i,t}^{\pm}=\mp K_I\,\frac{\delta_{i,t}-\delta_i^{(0)}}{\delta_i^{(0)}} \tag{6}$$

which corresponds to the elastic contribution, analogous to Eq. (5) for the grain.

The equation of motion for the two subnodes is then

$$\rho L_n\ddot{u}^{\pm}=F^{\pm}-\gamma\dot{u}^{\pm}+f^{\pm}+\mathfrak{I}^{\pm}. \tag{7}$$

By subtracting and summing these equations, we obtain the following:

The differential equation of the state evolution of the interstice (describing the hysteretic loop)

$$\rho L_n\ddot{\delta}=P-\gamma\dot{\delta}+2f+\mathfrak{I}^{+}-\mathfrak{I}^{-}. \tag{8}$$

The differential equation describing the pulse propagation

$$\rho L_n\ddot{y}=F-\gamma\dot{y}, \tag{9}$$

where

$$P=F^{+}-F^{-}, \tag{10}$$

$$y=(u^{+}+u^{-})/2, \tag{11}$$

$$F=(F^{+}+F^{-})/2. \tag{12}$$

1. Rigid interstice case

In a time interval $(t,t+1)$ in which the interstice remains rigid, i.e., $\delta_{t+1}=\delta_t$, it follows:

$$\dot{\delta}\approx\frac{\delta_{t+1}-\delta_{t-1}}{2\tau}=\frac{\delta_t-\delta_{t-1}}{2\tau}=\frac{\Delta\delta_{t-1}}{2\tau}, \tag{13}$$

$$\ddot{\delta}\approx\frac{\delta_{t+1}-2\delta_t+\delta_{t-1}}{\tau^2}=-\frac{\Delta\delta_{t-1}}{\tau^2}, \tag{14}$$

where we have applied the usual first order finite difference formalism together with the definition of the forward difference operator

$$\Delta y_k=y_{k+1}-y_k. \tag{15}$$

From Eqs. (6), (8), and (9), it follows

$$f=-\frac{P}{2}-\frac{a}{2}\Delta\delta_{t-1}+K_I(\delta-\delta^{(0)}), \tag{16}$$

where

$$a=\frac{1}{2\tau}\left(\frac{2\rho L_n}{\tau}-\gamma\right). \tag{17}$$

Note that if δ never changes (permanently rigid interface), $\Delta\delta_{t-1}=0$ and $\delta=\delta^{(0)}$ at all times, and therefore

$$f=-P/2 \tag{18}$$

as in Ref. 15. In this case, $u^{+}=u^{-}$ at each time.

2. Classical interstice case

When the interstice is not rigid, the arrival of an external excitation may change its length. Then, at least locally, we must assume that the material is undergoing a change. Accordingly, we modify Eq. (16) by multiplying the three terms on the right-hand side by three bond ''quality'' parameters q, q', and q'' (each of them less or equal to unity), which allow us to specify the quality of the interface bond at the time t:

$$f=-q\frac{P}{2}-q'\frac{a}{2}\Delta\delta_{t-1}+q''K_I(\delta-\delta^{(0)}). \tag{19}$$

In the general case of a ''classical'' interstice, q, q', and q'' are assumed to be constant, but more generally they may depend on the stress in a continuous and reversible way. The rigid interstice phase is recovered by placing all values equal to unity.

Substituting Eq. (19) into Eq. (8), we obtain

$$\rho L_n\ddot{\delta}=rP-\gamma\dot{\delta}-q'a\Delta\delta_{t-1}-2r''K_I(\delta-\delta^{(0)}), \tag{20}$$

where $r=1-q$, $r''=1-q''$. Equation (9) remains unaffected, because it does not involve the internal forces.

Following Eq. (20), the overall elastic properties of the GBG cells are defined by an effective elastic constant, which is a function of the elastic constants of the grain and bond, and of the (instantaneous) values of the bond quality parameters

$$K_{\text{eff}}=\Phi(K_g,K_i,q,q',q''). \tag{21}$$

Since $u^{\pm}=y\pm\delta/2$, we obtain from Eqs. (9) and (20),

$$2\rho L_n \ddot{u}^{\pm} = (1+r)F^{\pm} + (1-r)F^{\mp} - 2\gamma \dot{u}^{\pm} \mp q' a(\Delta u^{+}_{t-1} - \Delta u^{-}_{t-1}) \mp 2r''(u^{+} - u^{-} - \delta^{(0)}). \quad (22)$$

From Eq. (22) and by assuming that L_n and τ are chosen in order to assure optimal convergence,

$$\frac{2L_n}{\tau} = \sqrt{\frac{K_g}{\rho}}, \quad (23)$$

it follows:

$$Bu^{\pm}_{t+1} = (1+r)u^{\mp}_{i\pm1} + (1-r)u^{\pm}_{i\mp1} - 2Au^{\pm}_{t-1} + q'A(u^{\pm}_{t-1} - u^{\mp}_{t-1}) + E(u^{\pm} - u^{\mp}) \pm \frac{2K_i r''}{C}\delta^{(0)}, \quad (24)$$

where

$$C = \frac{2L_n\rho}{\tau^2}, \quad B = 1 + \frac{\gamma}{C\tau}, \quad A = 1 - \frac{B}{2}, \quad E = 1 - r - q'A - \frac{2K_I r''}{C}. \quad (25)$$

We remark here that, when the linear attenuation is not negligible, better convergence is obtained by choosing a frequency dependent time step[18]

$$\frac{2L_n}{\tau} = \sqrt{\frac{\rho}{K_g}}\sqrt{\frac{1+\sqrt{1+4\gamma^2/(\omega^2\rho^2(2L_n)^2)}}{2}}. \quad (26)$$

Equations (25) needs to be correspondingly modified.

B. Nonclassical phase materials

In a classical phase material, the parameters q, q', and q'' at each grid point are smooth single valued functions of the stress. In a nonclassical material, the internal structure may vary discontinuously and nonuniquely as a function of the applied stress. The discontinuous or nonunique stress dependence may be due to various physical mechanisms, e.g., a redistribution of dislocations, crack activation (opening or closing) or frictional forces (jerks). In the case of nonlinear elastic materials it is reasonable to assume that these changes affect only the interstice region. The effects at the mesoscopic–microscopic scale may be conveniently modeled by introducing a more complex dependence of the bond quality parameters q, q', and q'' on the local applied pressure. To describe the dependence of the bond quality parameters on the externally applied driving pressure in a nonclassical phase, we apply an approach similar to the one of Ref. 10, as described in Sec. II. We assign a pair of pressure parameters P_0 and P_c to each GBG cell ($P_0 \leqslant P_c$). When the local pressure applied to the interstice reaches the value P_c, we allow the bond quality parameters to switch from their initial values to unity, i.e., the bond becomes rigid for $P > P_c$. Conversely, when P decreases below P_0, the bond-quality parameters are switched to a value less than unity. The protocol for the bond quality parameter q as a function of the local pressure P is schematized in Fig. 5. Since q' affects only the wave attenuation, which is not relevant in the present context, we keep for simplicity $q' = 1$ at all times. Likewise, for simplicity, we set $q'' = q$ at all pressures. Other choices of protocol are, of course, possible and might be more suitable in general or in particular situations.

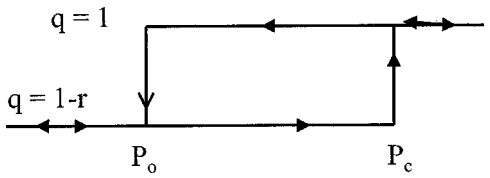

FIG. 5. Representation of the protocol for the dependence of the bond quality factor q on the applied pressure.

In the above described protocol, the specimen is represented as a sequence of GBG cells, each defined by a pair of activation pressures and by an initial bond state configuration. If $P \geqslant P_c$ or $P \leqslant P_0$, there is only one possible state, rigid or elastic, respectively. In the pressure range $P_0 < P < P_c$ two different states are possible, depending on the activation history of the GBG. The distribution of the pair of values (P_0, P_c), represented by the density $\rho_{\mathrm{NC}}(P_0, P_c)$ of nonclassical GBG cells (hysteretic and reversible elastic units), can be obtained by inversion of quasistatic stress–strain measurements.[19,20]

The initial q distribution (at $t = 0$) is strongly affected by the previous activation history of the specimen. In the following the specimen is assumed to be, at the time $t = 0$, com-

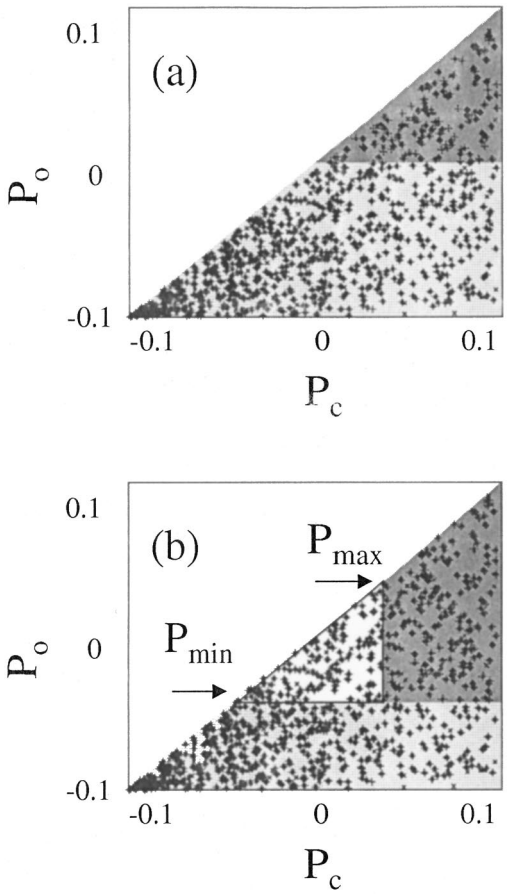

FIG. 6. PM space representation. Each dot represents one HEU or REU. (a) Specimen initially at zero pressure. Units in the dark gray and light gray areas are initially soft or rigid, respectively; (b) specimen under an external sinusoidal driving pressure between $p_{\min}$ and $p_{\max}$. Units in the dark gray, light gray, and white areas are permanently soft, permanently rigid and active, respectively.

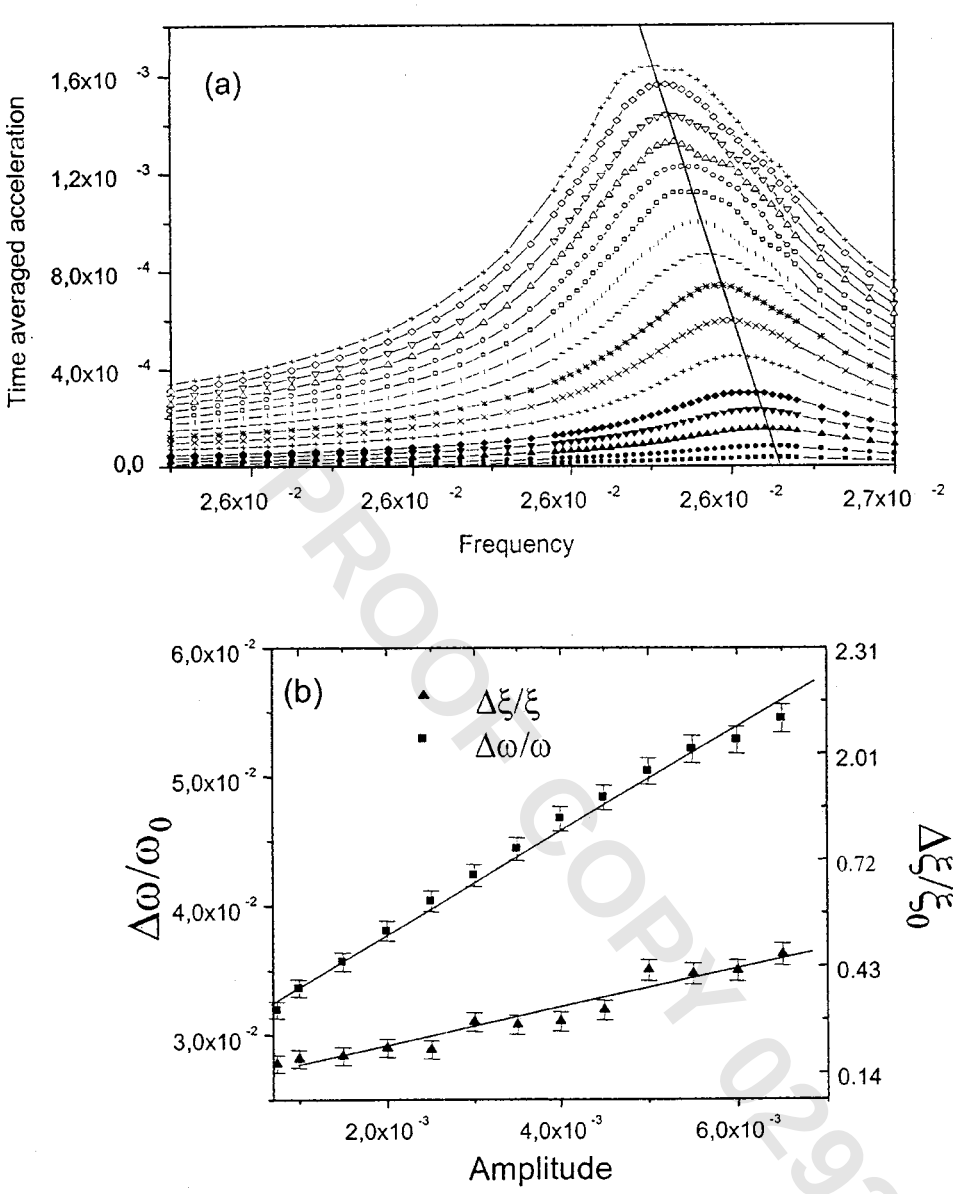

FIG. 7. Result of a resonant dynamic experiment. (a) Time averaged acceleration versus frequency for different driving amplitudes. (b) Normalized frequency shift and attenuation vs output wave amplitude at resonance.

pletely relaxed, i.e., kept at atmospheric pressure ($P=0$ after proper rescaling) and constant temperature for a sufficiently large time interval. The initial conditions then corresponds to the low energy ''equilibrium state'' produced by applying an oscillatory field amplitude slowly decreasing from a very large value to zero.[21] Assuming that random transitions between the elastic and rigid states occur when the applied pressure falls between the opening and closing pressures (see Ref. 9 for more details about the relaxation process), the following initial conditions apply:

$$\begin{aligned} &q=1 \quad \text{if } P_0<0 \quad \text{and } P_c<0,\\ &q=1-r \quad \text{if } P_c>0 \quad \text{and } P_0>0,\\ &q=1 \quad \text{with probability } p_e/(p_r+p_e)\\ &\qquad \text{if } P_c>0 \quad \text{and } P_0<0,\\ &q=1-r \quad \text{with probability } p_r/(p_r+p_e), \end{aligned} \tag{27}$$

where p_e and p_r are the transition probabilities from the elastic to the rigid state and vice versa.

Once the initial configuration is specified and the forcing protocol defined, the iteration equations (24) yield the temporal evolution of the system.

IV. SIMULATIONS OF NONLINEAR RESONANT BAR EXPERIMENTS

In the following we focus our attention on a resonant bar experiment performed on a typical material exhibiting nonclassical nonlinearity.[1] We assume that a rod-shaped specimen is equipped with a transducer generating monochromatic waves of excitation amplitude A_d attached at one end and with an accelerometer attached to the other end. The frequency f_d is swept through the fundamental resonance mode f_0 of the specimen and the time averaged acceleration amplitude A_r (in stationary conditions) is recorded. This procedure of resonance curve tracking is repeated for several different levels of excitation.

In the simulation approach, each elastic unit (HEU or REU) corresponds to a point in the PM space [see Fig. 6(a)]. The dark and light gray areas in the plot correspond to ini-

tially soft and rigid interstices, respectively. In the stationary state of a resonance, the actual pressure P for each HEU/REU oscillates between a minimum and a maximum pressure ($P_{\min}$ and $P_{\max}$, respectively), depending on the external excitation level and its location in the bar [see Fig. 6(b)]. If the HEU/REU is situated within the activation triangle (the PM space area bounded by the diagonal $P_0=P_c$ and the lines $P_0=P_{\min}$ and $P_c=P_{\max}$), the nonlinear properties are activated by the forcing (white area in the plot). As a consequence, the bond will change during the excitation process between rigid and soft.

In all the simulations arbitrary units have been chosen. The values of the parameters are $\rho=1$, $K_g=1$, $K_i=3$, $2L_n=1$, $\delta^{(0)}=1$, $\gamma=0.0001$, $p_e=0.0001$, and $p_r=0$. Simulations have been performed considering 1000 grains. Stationary conditions were usually reached in about 40 round trips of the wave. Results are qualitatively independent from the choice of the transition rates p_r and p_e, provided $p_r<p_e \ll 1$ (see also Ref. 9). Similar behaviors are found for the fundamental resonance and for higher modes.

Figure 7 illustrates a typical numerical simulation of the resonant bar experiment (simulations are performed without letting the system relax to the original initial conditions after each sweep). The time averaged acceleration amplitude on the free edge is plotted vs frequency for several driving amplitudes in Fig. 7(a). From Fig. 7(a) (using a Lorentzian fit), one can determine the resonance frequency and its amplitude. The width of the resonance curve is a measure of the attenuation. In the case of skewed resonance curves the attenuation can be obtained by means of the RTMF method

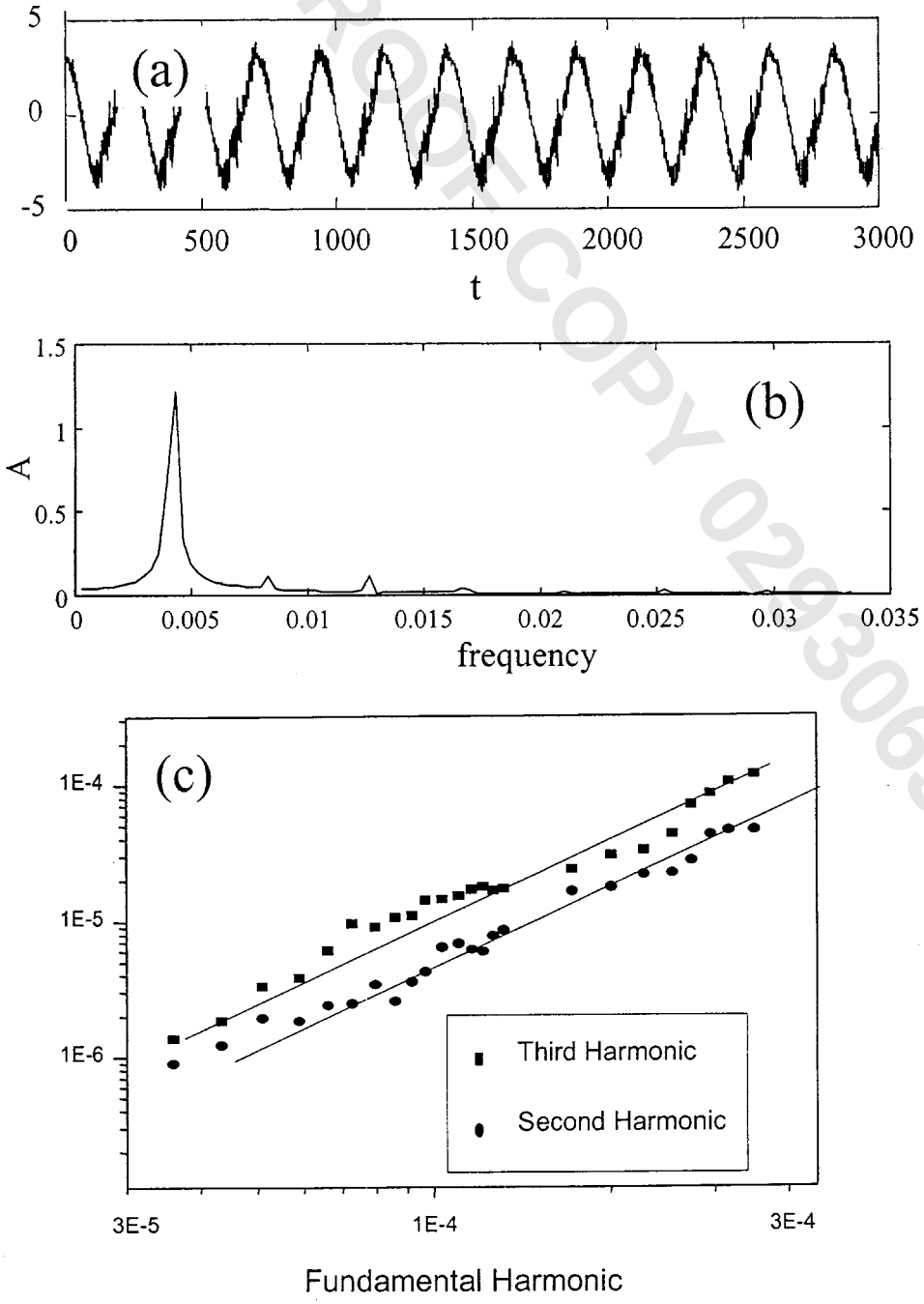

FIG. 8. Generation of higher order harmonics. (a) Temporal signal (acceleration versus time); (b) fast Fourier transform of the signal; (c) amplitudes of the second and third harmonics vs the fundamental one.

proposed by Smith *et al.*[22] The relative changes of frequency and attenuation (defined as the half-width of the Lorentzian) vs the resonance amplitude are shown in Fig. 7(b). Both of them display a linear dependence on the amplitude of the output acceleration in resonance, although an initial saturation is observed for the resonance frequency shift, in agreement with experimental data.[23]

The temporal signal in resonance is shown in Fig. 8(a) for a given driving amplitude. The signal (perfectly sinusoidal in the linear case or at very low driving amplitudes) is distorted due to the nonlinearity. The triangular shape betrays the hysteretic behavior of the system. The fast Fourier transform (FFT) of the signal is illustrated in Fig. 8(b). As expected, higher order harmonics (both even and odd) are generated. Even harmonics arise in the present model, since all HEU and REU contribute to both hysteretic and non hysteretic nonlinearity. In fact, the bimodulus feature in $P=P_c$ (see Fig. 4), or more precisely the modulus jump, leads to the formation of higher order harmonics (at any order).

Finally, in Fig. 8(c) we analyze the dependence of the second and third order harmonics on the amplitude of the fundamental one in a log–log plot. Both curves have slope two, in agreement with experimental data. We recall that the expected slopes in the classical nonlinear case are two and three for the second and third harmonics, respectively. The ratio between the amplitudes of the second and third order harmonics depends strongly on the choice of the parameters, but is always less than one. The ratio may range from close to one to almost zero, in agreement with experimental observations on different materials.[24]

V. CONCLUSIONS

We have presented a numerical simulation approach to the study of nonclassical nonlinear effects induced by soft inclusions in a hard matrix. Typical examples of soft inclusions are the interstices among grains in a rock. In our approach they are represented by means of lattice units including portions of the adjoining grains. For each elastic unit we assume that all the nonlinearity is included in the interstice region. The nonclassical nonlinear behavior of the unit arises from transitions between a rigid and a soft state (or vice versa).

The above nonclassical micromodel has been implemented in the framework of a local interaction simulation approach (LISA). As a result it has been possible to reproduce, at least qualitatively, most of the nonclassical nonlinear effects, which have been discovered in recent years in quasistatic and in resonant dynamics experiments. Some of these results are included in the present paper.

A very important effect, the so-called ''slow dynamics,'' which gives rise to a logarithmic increase with time of the resonance frequency and amplitude in a resonant dynamics experiment when the driving force is released, has been ignored, since it requires the further inclusion of additional mechanisms.[9]

Another very important extension of the model concerns the possibility of applying it to the analysis of local or diffused damage.[25] By indentifying the appropriate changes in the density representation of HEU's and REU's, the model can be utilized as a powerful tool for nondestructive evaluation in a large variety of structural or earth materials.

The micromodel and protocol, which have been used to describe the local elasticity, represent, of course, only one of many possible alternatives.[26] The main purpose of the present work is to present a method, which is flexible enough to allow one to adopt any plausible model (even if it includes complex local interaction mechanisms) and to illustrate its implementation by means of a model, which seems to us to be particularly appealing. Another goal is to elicit more detailed experiments, in order to discriminate conclusively between the variety of plausible models and solicit suggestions based on basic mechanisms at the molecular dynamics level.

ACKNOWLEDGMENTS

The work was supported by the INFM Parallel Computing Initiative and by MURST (prot. NM02328989, Italy). The authors also acknowledge support by a University Collaborative Research Program of The Institute of Geophysics and Planetary Physics at the Los Alamos National Laboratory, NM, USA, by the US DOE Office of Basic Energy Science, and by the ESF–PESC program NATEMIS. The authors are grateful to E. Smith (Santa Fe' Institute, NM) and D. Iordache (Univ. of Bucharest, Romania) for fruitful discussions.

[1] R. A. Guyer and P. A. Johnson, ''Nonlinear mesoscopic elasticity: evidence for a new class of materials,'' Phys. Today **52**, 30–36 (1999).
[2] R. A. Guyer, J. A. Tencate, and P. A. Johnson, ''Hysteresis and the dynamic elasticity of consolidated granular materials,'' Phys. Rev. Lett. **82**, 3280–3283 (1999).
[3] J. A. TenCate, K. E.-A. Van Den Abeele, T. J. Shankland, and P. A. Johnson, ''Laboratory study of linear and non linear elastic pulse propagation in sandstone,'' J. Acoust. Soc. Am. **99**, 3334–3345 (1996).
[4] L. D. Landau and E. M. Lifshitz, *Theory of Elasticity* (Pergamon, Oxford, 1986).
[5] K. Van Den Abeele, ''Elastic pulsed wave propagation in media with second-or higher order non linearity,'' J. Acoust. Soc. Am. **99**, 3334–3345 (1996).
[6] R. A. Guyer, K. R. McCall, and G. N. Boitnott, ''Hysteresis, discrete memory and nonlinear wave propagation in rock: a new paradigm,'' Phys. Rev. Lett. **74**, 3491–3494 (1994).
[7] J. A. TenCate and T. J. Shankland, ''Slow dynamics in nonlinear elastic response of Berea sandstone,'' Geophys. Res. Lett. **23**, 3019–3022 (1996).
[8] J. A. TenCate, E. Smith, and R. A. Guyer, ''Universal slow dynamics in granular solids,'' Phys. Rev. Lett. **85**, 1020–1024 (2000).
[9] M. Scalerandi, P. P. Delsanto, and P. A. Johnson, ''Stress induced conditioning and thermal relaxation in the simulation of quasi-static compression experiments,'' J. Phys. D **36**, 288–293 (2003); M. Scalerandi and P. P. Delsanto, ''Modelling nonlinearity, conditioning and slow dynamics in mesoscopic elastic materials,'' Phys. Rev. B (submitted).
[10] J. D. Holcombe, ''Memory, relaxation and microfracturing in dilatant rocks,'' J. Geophys. Res. B **86**, 6235–6248 (1981); K. R. McCall and R. A. Guyer, ''A new theoretical paradigm to describe hysteresis, memory and nonlinear elastic wave propagation in rock,'' Nonlinear Processes Geophysics **3**, 89–101 (1996).
[11] K. Van Den Abeele, P. A. Johnson, R. A. Guyer, and K. R. McCall, ''On the quasi analytic treatment of hysteretic nonlinear response in elastic wave propagation,'' J. Acoust. Soc. Am. **101**, 1885–1898 (1997).
[12] F. Cleri, ''Atomic and electronic structure of high energy grain boundaries in silicon and carbon,'' Comput. Mater. Sci. **20**, 351–362 (2001).
[13] F. Cleri, S. Yip, D. Wolf, and S. R. Phillpot, ''Atomic-scale mechanism of crack-tip plasticity: Dislocation nucleation and crack-tip shielding,'' Phys. Rev. Lett. **79**, 1309–1312 (1999).
[14] P. P. Delsanto, R. Mignogna, M. Scalerandi, and R. Schechter, ''Simulation of ultrasonic pulse propagation in complex media,'' in *New Perspectives on Problems in Classical and Quantum Physics*, edited by P. P.

Delsanto and A. W. Saenz (Gordon & Breach, New Delhi, 1998), Vol. 2, pp. 51–74.
[15] P. P. Delsanto *et al.*, ''Connection machine simulation of ultrasonic waves propagation I: the 1-D case,'' Wave Motion **20**, 295 (1994).
[16] P. P. Delsanto and M. Scalerandi, ''A spring model approach for the simulation of wave propagation across imperfect interfaces,'' J. Acoust. Soc. Am. **104**, 2584–2591 (1998).
[17] M. Scalerandi, E. Ruffino, P. P. Delsanto, P. A. Johnson, and K. Van Den Abeele, ''Simulation of acoustic wave propagation in non classical, non linear mesoscopic media, in *Review of Progress in Quantitative Non Destructive Evaluation*, edited by D. O. Thompson and D. E. Chimenti, Conf. Proc. Vol. 19B (AIP, Melville, NY, 2000), 1393–1399.
[18] R. Courant, K. Friedrichs, and H. Lewy, ''Uber die partiellen differenzgleichungen der mathematischen physik (Partial differential equations in mathematical physics),'' Math. Ann. **100**, 32–38 (1928); D. Iordache *et al.*, ''Simulation of the wave propagation in 1-D Zener attenuative media,'' Nuovo Cimento B **114**, 1413–1426 (1999).
[19] E. Ruffino and M. Scalerandi, ''Analysis of the elastic behavior of nonclassical non linear mesoscopic materials in quasi-static experiments,'' Nuovo Cimento B **115**, 645–652 (2000).
[20] P. A. Johnson and P. N. J. Rasolofosaon, ''Manifestation of non linear elasticity in rock,'' Nonlinear Proc. Geophys. **3**, 89–95 (1996).
[21] G. Bertotti, ''Energetic and thermodynamic aspects of hysteresis,'' Phys. Rev. Lett. **76**, 1739–1742 (1996); G. Zarand *et al.*, ''Using hysteresis for optimization,'' *ibid.* **89**, 150201 (2002).
[22] D. E. Smith and J. A. TenCate, ''Sensitive determination of nonlinear properties of Berea sandstone at low strains,'' Geophys. Res. Lett. **27**, 1985–1988 (2000).
[23] P. A. Johnson *et al.*, ''Resonance and nonlinear elastic phenomena in rock,'' J. Geophys. Res., [Solid Earth] **101**, 11553–64 (1996). See in particular Fig. 5.
[24] B. Zinszner *et al.*, ''Influence of change in physical state on elastic nonlinear response in rock,'' J. Geophys. Res., [Solid Earth] **102**, 8105–8120 (1997) (see in particular Fig. 13); L. A. Ostrowsky and P. A. Johnson, ''Dynamic nonlinear elasticity in geomaterials,'' Riv. Nuovo Cimento **24**, 1–46 (2001) (see in particular Fig. 10); K. Van den Abeele *et al.*, ''Nonlinear elastic wave spectroscopy (NEWS) techniques to discern material damage, Part 1: nonlinear wave modulation spectroscopy,'' Res. Nondestruct. Eval. **12**, 17–30 (2000) (see in particular Figs. 4 and 7).
[25] K. Van Den Abeele, P. A. Johnson, J. Carmeliet, and A. Sutin, ''Microdamage diagnostics using non linear elastic wave spectroscopy,'' NDT & E Int. **34**, 239–248 (2001).
[26] P. P. Delsanto, V. Agostini, M. Scalerandi, and P. A. Johnson, ''Phenomenology and modeling of damaged mesoscopic materials,'' Proceedings of EuroMech Conference, Prague, 2000; B. Capogrosso Sansone and R. A. Guyer, Phys. Rev. B (in press).